ORIGINAL

Clinical application of dynamic ^{18}F-fluorodeoxyglucose positron-emission tomography/computed tomography in the differential diagnoses of musculoskeletal lesions

Takayoshi Shinya[1, 2, 3], Yoichi Otomi[1], Toshihiko Nishisho[4], Bettina Beuthien-Baumann[2], Saho Irahara[1], Michiko Kubo[1], Hideki Otsuka[5], Yoshimi Bando[6], Koichi Sairyo[4], and Masafumi Harada[1]

[1]Department of Radiology, Tokushima University Hospital. 2-50-1, Kuramoto-cho, Tokushima City, Tokushima, 770-8503, Japan, [2]Division of Radiology, German Cancer Research Centre (DKFZ), Im Neuenheimer Feld 280, 69120, Heidelberg, Germany, [3]Department of Diagnostic and Therapeutic Radiology, Kawasaki Medical School General Medical Center, 2-6-2 Nakasange, Kita-ku, Okayama City, Okayama, 700-8505, Japan, [4]Department of Orthopedics, Institute of Biomedical Sciences, Tokushima University Graduate School, 3-18-15 Kuramoto-cho, Tokushima-city, 770-8503, Tokushima, Japan, [5]Department of Medical Imaging/Nuclear Medicine, Institute of Biomedical Sciences, Tokushima University Graduate School. 2-50-1, Kuramoto-cho, Tokushima City, Tokushima, 770-8503, Japan, [6]Division of Pathology, Tokushima University Hospital. 2-50-1, Kuramoto-cho, Tokushima City, Tokushima, 770-8503, Japan

Abstract : We aimed to assess the differential diagnostic efficacy of dynamic F-18 fluorodeoxyglucose (FDG) positron emission tomography/computed tomography (PET/CT) and to evaluate the appropriate scan timings for diagnosis of musculoskeletal lesions (MSLs). Dynamic scans (5–15 [phase 1], 15–25 [phase 2], and 25–35 [phase 3] min after F-18 FDG injection) and dual-time-point scans (1 and 2 h after injection) were acquired for 23 MSLs [4 benign MSLs (BMSLs). 10 primary malignant musculoskeletal tumors (PMMSTs), and 9 metastatic musculoskeletal tumors (MMSTs)]. We compared the maximum standardized uptake values (SUVmax) and corresponding retention indices for dynamic (RI-SUVdyn) and dual-time-point (RI-SUVdual) scans and evaluated diagnostic efficacy using receiver operating characteristic (ROC) curve analyses. The SUVmax gradually decreased or was almost identical with minimal fluctuation in 3 BMSLs and 1 PMMST. SUVmax increased over time after phase 2 in 18 malignant MSLs (MMSLs). There were significant differences in SUVmax (for all time phases) and RI-SUV dual between BMSLs and MMSLs and between PMMSTs and MMSTs. In the ROC analyses, the areas under the curve for SUV in phases 2 and 3 were highest for differentiating BMSLs from MMSLs and PMMSTs from MMSTs, respectively. Dynamic F-18 FDG PET/CT is valuable for diagnosis of musculoskeletal lesions. J. Med. Invest. 68 : 96-104, February, 2021

Keywords **:** *bone and soft tissue tumors, dynamic scan, musculoskeletal lesion, positron emission tomography computed tomography, sarcoma*

INTRODUCTION

Bone and soft tissue tumors have several physiological, biochemical, and genetic characteristics. In clinical practice, orthopedic surgeons and radiologists encounter musculoskeletal lesions (MSLs) of unknown origin. It is important to differentiate the benign and malignant lesions to justify performing a biopsy and initiating optimal treatment. However, differentiating between the lesions can be difficult without typical imaging findings, leading to a diagnostic dilemma with respect to benign MSLs (BMSLs), primary malignant musculoskeletal tumors (PMMSTs), and metastatic musculoskeletal tumors (MMSTs). In patients with typical imaging findings or with a metastatic primary site, MSLs can be diagnosed using conventional morphologic imaging and metabolic imaging modalities, such as plain radiography, computed tomography (CT), and magnetic resonance imaging (MRI). Functional imaging techniques, including Tl-201 scintigraphy, Tc-99m (V) dimercaptosuccinic acid (DMSA) scintigraphy, and positron emission tomography (PET), are used to obtain complementary information in specific clinical situations (1-6). However, the morphological appearance and metabolism of these tumors overlap, and a reliable imaging method is not available to date.

Recently, several studies have reported absolute PET quantification of physiological parameters using tracer kinetic modeling (7-12). Dynamic PET imaging is expected to aid in understanding the pathophysiological mechanisms of diseases and extracting physiological or biochemical parameters via tracer kinetics. Despite its value, dynamic PET imaging with kinetic model analysis is primarily confined to research centers and not used in busy clinical settings, mainly because it is technically demanding (13). Technical developments in ^{18}F-fluorodeoxyglucose (FDG) PET/CT using dynamic scans have enabled the estimation of perfusion-dependent FDG uptake and metabolic activity in various tumors (14-18). Recent studies have shown that dynamic PET/CT in list-mode, without kinetic model analysis, can be a simple tool for predicting pathological and clinicopathological tumor characteristics (14, 15, 19, 20). However, to our knowledge, no studies have reported the diagnostic performance of dynamic ^{18}F-FDG PET/CT in list-mode for differentiation between BMSLs and malignant musculoskeletal lesions (MMSLs), and between PMMSTs and MMSTs.

The present study aimed to assess the efficacy of early dynamic PET/CT scanning with list-mode and dual-time-point (DTP) PET/CT scanning to differentiate between malignant and benign lesions in patients with newly diagnosed MSLs. We also compared the diagnostic capacity of dynamic PET/CT and DTP PET/CT for MMSLs and identified the most appropriate imaging phase for differentiating between the MSLs.

Received for publication October 5, 2020 ; accepted November 20, 2020.

Address correspondence and reprint requests to Takayoshi Shinya, Department of Diagnostic and Therapeutic Radiology, Kawasaki Medical School General Medical Center, 2-6-2 Nakasange, Kita-ku, Okayama City, Okayama, 700-8505, Japan and Fax : +81-86-232-8343.

PATIENTS AND METHODS

All procedures performed in this study that involved human participants were in accordance with the ethical standards of the institutional research committee and with the 1964 Helsinki Declaration and its later amendments or comparable ethical standards. This study was approved by the Ethics Committee of Tokushima University Hospital (Approval number 2606). Informed consent was obtained from all participants included in the study.

Study population

We included patients with MSLs of unknown origin, for whom the diagnosis was finally determined by pathological examinations. Additional inclusion criteria were as follows : no therapy for MSLs before PET/CT and no history of malignancy within the last 3 years.

^{18}F-FDG PET/CT procedures

Before intravenous injection of ^{18}F-FDG (8.0×10^{-5} Ci/kg of body weight), all patients fasted for > 5 h and achieved a blood glucose level of <150 mg/dL. PET/CT was conducted using a single PET/CT system (Discovery PET/CT 710 ; GE Healthcare, Chicago, IL, USA) enabled with list-mode data acquisition function and four-dimensional data acquisition (i.e., dynamic scanning). The protocol included 3 acquisitions : (1) dynamic PET acquisition (limited to the single-bed position), (2) low-dose CT scan centered on the largest MSL of interest and initiated 5 min after ^{18}F-FDG injection, and (3) DTP static PET/CT scan of the torso (lasting approximately 12–16 min). All participants underwent dynamic and DTP PET/CT examinations with their upper limbs down.

During the first acquisition, low-dose CT was performed to determine PET attenuation correction, anatomical information, and image fusion. During the second acquisition, dynamic ^{18}F-FDG PET/CT was performed as list-mode continuous scanning, beginning 5 min after FDG bolus injection and continuing for 30 min, with every measured value stored as raw data with the exact time stamp. The dynamic series were acquired with the field of view over the lesions of interest (limited to a single-bed position, with longitudinal coverage of 15.042 cm). Patients were asked to lie motionless during dynamic scanning. We subsequently reconstructed the data as 3 frames at 600-s intervals. The list-mode files were reconstructed on the PET/CT scanner using three-dimensional, attenuation-weighted, ordered-subset, expectation maximization, with 2 iterations and 16 subsets (VUE Point FX ; GE Healthcare), a 4-mm post-reconstruction Gaussian filter, attenuation image segmentation, and a 192 × 192-pixel matrix. The patient then waited in a waiting room before returning to the scanner for the subsequent procedure, conducted 60 min after tracer injection.

The DTP PET/CT scanning region for the 1-h early scan encompassed the body from the skull vertex to the knee, and for the 2-h delayed scan, it encompassed the field of view over the MSL of interest. Before conducting DTP PET/CT, a second low-dose CT scan was immediately performed for attenuation correction over the shooting range. The early and delayed PET scans were acquired at 8- and 4-bed positions and for 120 and 180 s, respectively. For each scan, we used the same image reconstruction method used for dynamic FDG PET.

PET/CT image analysis

The dynamic and DTP PET/CT images were reviewed by 2 nuclear medicine physicians (with >15 years of experience) blinded to all clinical, pathological, and other imaging findings. In case of disagreement, they reached a consensus via discussion. Any obvious foci within the MSL that showed increased FDG uptake relative to the surrounding tissue, which could not be explained by the physiological uptake of the tracer in these sites, were considered positive.

Using the PET/CT images, we carefully placed the volume of interest (VOI) on the MSL to exclude FDG accumulation in the normal tissue and large vessels, and circular VOIs were drawn to encompass each lesion contour on transaxial images. These VOIs were placed after consensus was reached between the 2 nuclear medicine physicians.

For the semiquantitative analysis of FDG uptake, we adopted the standardized uptake value (SUV), which was calculated, as follows :

> SUV = concentration of radioactivity (Ci/kg) × [lean body mass (kg)/injected radioactivity (Ci)]

To minimize partial-volume effects, SUVmax within VOIs was used. SUVmax was measured for each dynamic phase (SUV1, 5–15 min ; SUV2, 15–25 min ; and SUV3, 25–35 min), the 1-h early phase (SUV4), and the 2-h delayed phase (SUV5). Furthermore, we calculated the retention index (RI)-SUVmax from the SUVmax as follows :

> Retention index of the dynamic phase SUVmax (RI-SUVdyn [%]) = (SUV3 – SUV1) × 100/SUV1
>
> Retention index of DTP SUV (RI-SUVdual [%]) = (SUV5 [delayed scan] – SUV4 [early scan]) × 100/SUV4 (early scan).

In addition, we calculated the mean SUV (SUVmean) for each subject.

The maximal diameter of each tumor lesion was measured on axial low-dose CT images.

Statistical analysis

To analyze differences in SUVmax among different phases, RI-SUVdyn, and RI-SUVdual, we employed the Mann–Whitney U-test for comparisons between BMSLs and MMSLs and the Kruskal–Wallis test followed by the Steel–Dwass test for comparisons among BMSLs, PMMSTs, and MMSTs.

If the Mann–Whitney U-test and Kruskal–Wallis test followed by the Steel–Dwass test revealed a significant difference in each index among the groups, we performed additional receiver operating characteristic (ROC) curve analyses for SUVmax and RI-SUVmax to evaluate the predictive performance of these indices in differentiating between MSL types. Discriminatory ability was assessed using the area under the ROC curve (AUC) values. We determined the optimal cut-off values that maximized the sensitivity and specificity for each index and the corresponding sensitivity, specificity, positive predictive value (PPV), negative predictive value (NPV), and accuracy. Significant differences between 2 AUC values were assessed using Delong's test. All statistical analyses were conducted using EZR version 1.37 (Saitama Medical Center, Jichi Medical University, Saitama, Japan ; available at www.jichi.ac.jp/saitama-sct/SaitamaHP.files/statmedEN.html), a graphical user interface for R (The R Foundation for Statistical Computing, Vienna, Austria) (21). Statistical significance was set at $p < 0.05$.

RESULTS

Patient and tumor characteristics

The patient and tumor characteristics are presented in Table 1. Between January 2016 and October 2016, 19 patients met the inclusion criteria and underwent dynamic and DTP ^{18}F-FDG

PET/CT (12 men, 7 women ; age [mean ± SD] 69.21 ± 10.40, range 37–81 years). Twenty-three lesions were identified as bone and soft tissue lesions on PET/CT evaluations (15 soft tissue, 8 bone). The MSLs were classified according to the WHO Classification of Tumours of Soft Tissue and Bone, Fourth Edition (22), by pathologists blinded to the PET results. Histopathologically, 4 lesions (17%) were classified as BMSLs, 10 (44%) as PMMSTs (soft tissue tumors : 7 grade [G] 2 ; bone tumors : 2 G2 and 1 G3), and 9 (39%) as MMSTs. Of the 4 bone metastases, 3 were solitary bone tumors.

The tumor diameters ranged from 20 to 245 mm, with most lesions having a long-axis diameter of < 60 mm. There was no significant between-group difference in the tumor size ($p = 0.117$).

Visual evaluation

All MMSLs and 2 BMSLs were FDG-positive on all dynamic phases and the 1-h early and 2-h delayed phases. In contrast, one osteochondroma was FDG-negative on all dynamic phases and the 1-h early and 2-h delayed phases, and another osteochondroma was negative on the dynamic first and second phases but positive on the dynamic third phase and the 1-h early and 2-h delayed phases.

SUVs and RI-SUVmax

SUVmax, RI-SUVmax, and SUVmean values are summarized in Tables 2 and 3. SUV1 was slightly higher than SUV2 for 2 BMSLs and 5 PMMSTs. For all other lesions, SUV2 was higher than SUV1. After the dynamic second phase, SUVmax gradually decreased or was near identical, with little fluctuation, for 3 BMSLs and 1 PMMST. In contrast, SUVmax increased over time after the dynamic second phase for 1 BMSL, 8 PMMSTs, and all MMSTs.

SUVmax for each time phase and RI-dual were significantly higher for MMSLs than for BMSLs ($p = 0.012$ for SUV1 ; $p = 0.00158$ for SUV2 ; $p = 0.00158$ for SUV3 ; $p = 0.00581$ for SUV4 ; $p = 0.00158$ for SUV5 ; $p = 0.00858$ for RI-dual). All SUVmax values were significantly higher for PMMSTs than for BMSLs ($p = 0.04771$ for SUV1 ; $p = 0.01621$ for SUV2 ; $p = 0.0162$ for SUV3 ; $p = 0.0195$ for SUV4 ; $p = 0.0162$ for SUV5). All metabolic parameters were significantly higher for MMSTs than for BMSLs ($p = 0.01355$ for SUV1 ; $p = 0.00548$ for SUV2, SUV3, SUV4, and SUV5 ; $p = 0.006851$ for RI-dyn ; $p = 0.0005479$ for RI-dual). SUVmax for each time phase and RI-dyn were significantly higher for MMSTs than for PMMSTs ($p = 0.0143$ for

Table 1. Characteristics of the patients and tumors

No./Patient Number/Age/Sex	Histology	Diagnosis with conventional imaging	Tumor site	Diameter (mm)
A. Benign musculoskeletal lesion				
1/1/80/male	Osteochondroma	Osteochondroma	Knee	20
2/2/68/male	Osteochondroma	Osteochondroma	Knee	40
3/3/67/male	Hematoma	Chronic expanding hematoma	Femur	245
4/4/77/male	Schwannoma	Schwannoma	Axilla	56
B. Primary malignant musculoskeletal tumor				
5/5/68/female	Chondroblastic osteosarcoma	Chondrosarcoma	Ilium	110
6/6/74/female	Dedifferentiated liposarcoma	Liposarcoma	Thigh	100
7/7/59/male	Pleomorphic leiomyosarcoma	Soft tissue sarcoma	Lower back	79
8/7/59/male	Pleomorphic leiomyosarcoma	Soft tissue sarcoma	Lower back	28
9/8/55/male	Myxofibrosarcoma	Soft tissue sarcoma	Thigh	57
10/9/81/male	Pleomorphic leiomyosarcoma	Soft tissue sarcoma	Back	48
11/10/65/female	Chondrosarcoma	Chondrosarcoma	Femur	190
12/11/37/female	Myxoid liposarcoma	Soft tissue sarcoma	Thigh	108
13/12/70/male	Myxofibrosarcoma	Soft tissue sarcoma	Shoulder	66
14/13/71/female	Chordoma	Chordoma	Sacrum	30
C. Metastatic musculoskeletal tumor				
15/14/79/male	SCC from lung cancer	Bone metastasis	Ilium (bone)	81
16/15/67/female	AC from lung cancer	Bone metastasis	Ilium (bone)	92
17/15/67/female	AC from lung cancer	Metastatic soft tissue tumor	Lower back (muscle)	24
18/16/78/female	AC from gastric cancer	Soft tissue sarcoma	Thigh (muscle)	79
19/17/71/male	SCC from hypopharyngeal cancer	Metastatic soft tissue tumor	Neck (muscle)	21
20/17/71/male	SCC from hypopharyngeal cancer	Metastatic soft tissue tumor	Neck (muscle)	28
21/17/71/male	SCC from hypopharyngeal cancer	Metastatic soft tissue tumor	Neck (muscle)	23
22/18/76/male	AC from lung cancer	Bone metastasis	Dorsal vertebra	28
23/19/72/male	Clear cell renal cell carcinoma	Bone metastasis	Dorsal vertebra	27

AC : adenocarcinoma, SCC : squamous cell carcinoma.

Table 2. SUVmax and RI-SUVmax values at each time-point in each group

	BMSL	MMSL	PMMST	MMST
SUV1	2.53 ± 0.75	4.48 ± 0.35	4.53 ± 0.26	5.72 ± 0.56
	(1.45–4.57)	(2.57–8.83)	(2.57–5.21)	(3.69–8.83)
SUV2	2.59 ± 0.41	5.29 ± 0.51	4.19 ± 0.71	6.58 ± 0.34
	(1.92–3.65)	(2.49–10.65)	(2.49–6.00)	(4.78–10.65)
SUV3	2.57 ± 0.37	6.29 ± 0.64	4.39 ± 0.45	7.58 ± 0.79
	(1.46–3.01)	(2.50–12.21)	(2.50–7.08)	(6.29–12.21)
SUV4	2.56 ± 0.97	9.66 ± 0.20	6.23 ± 1.01	10.77 ± 1.15
	(1.86–2.73)	(2.53–17.23)	(2.53–12.03)	(8.57–17.23)
SUV5	2.41 ± 0.23	11.37 ± 1.20	6.94 ± 1.33	13.96 ± 1.38
	(1.53–2.80)	(1.77–20.75)	(1.77–14.16)	(9.18–20.75)
RI-SUVdyn	-5.65% ± 14.08%	32.52% ± 6.16%	8.68% ± 6.91%	46.08% ± 3.94%
	(-47.48–32.52)	(-38.93–71.27)	(-38.93–45.68)	(32.52–71.27)
RI-SUVdual	-0.21% ± 3.75%	17.71% ± 4.67%	19.02% ± 6.63%	8.47% ± 6.82%
	(-17.74–3.70)	(-30.04–65.85)	(-30.04–48.15)	(4.65–65.85)

SUV, standardized uptake value ; RI-SUV, retention index of maximum standardized uptake value ; BMSL, benign musculoskeletal lesion ; MMSL, malignant musculoskeletal lesion ; PMMST, primary malignant musculoskeletal tumor ; MMST, metastatic musculoskeletal tumor ; dyn, dynamic ; dual, dual-time-point
Data are presented as median ± standard error of the mean. Data in parentheses represent the ranges.

Table 3. SUVmean at each time-point in each group

	BMSL	MMSL	PMMST	MMST
SUV1	1.76 ± 0.58	3.83 ± 0.26	3.61 ± 0.26	4.27 ± 0.41
	(1.11–3.59)	(2.09–6.20)	(2.09–4.28)	(2.40–6.20)
SUV2	2.11 ± 0.37	3.67 ± 0.36	3.19 ± 0.32	3.98 ± 0.59
	(1.34–3.09)	(1.89–7.56)	(1.89–5.42)	(3.22–7.56)
SUV3	2.10 ± 0.32	4.25 ± 0.39	3.08 ± 0.35	5.25 ± 0.53
	(1.27–2.67)	(2.10–8.33)	(2.10–5.84)	(4.01–8.33)
SUV4	2.05 ± 0.23	5.10 ± 0.55	4.0 ± 0.62	6.67 ± 0.65
	(1.23–2.24)	(2.13–10.18)	(2.13–8.81)	(4.86–10.18)
SUV5	1.54 ± 0.16	5.66 ± 0.70	4.10 ± 0.71	7.57 ± 0.92
	(1.06–1.78)	(1.43–14.38)	(1.43–9.81)	(5.62–14.38)

SUV, standardized uptake value ; BMSL, benign musculoskeletal lesion ; MMSL, malignant musculoskeletal lesion ; PMMST, primary malignant musculoskeletal tumor ; MMST, metastatic musculoskeletal tumor.
Data are presented as median ± standard error of the mean. Data in parentheses represent ranges.

SUV1 ; $p = 0.00145$ for SUV2 ; $p = 0.000605$ for SUV3 ; $p = 0.00898$ for SUV4 ; $p = 0.00898$ for SUV5 ; $p = 0.000815$ for RI-dyn).

Figures 1, 2, and 3 show representative dynamic and DTP ^{18}F-FDG PET/CT images of MMSTs, PMMSTs, and BMSLs. Figure 4 shows the change in median SUVmax values for each time phase per study group.

ROC curves and cut-off values for SUVmax and RI-SUVmax

Tables 4 and 5 show the threshold (i.e., cut-off) values for each parameter and the resulting sensitivity, specificity, PPV, NPV, and accuracy for discriminating between MMSLs and BMSLs and between MMSTs and PMMSTs.

For differentiating MMSLs from BMSLs, the cut-off values yielded the highest sensitivity of 94.7% and highest specificity of 100.0%, with PPV, NPV, and accuracy values of 94.7%, 100.0%, and 95.7%, respectively, for SUVmax analyses in the dynamic second phase. Compared with the AUC derived in all other ROC analyses, that for SUV2 was the largest at 0.987 ; however, Delong's test did not reveal any significant differences among the AUC values for all parameters ($p > 0.05$ for all).

For differentiating between the MMSTs and PMMSTs, the cut-off values yielded the highest sensitivity of 100.0% and highest specificity of 90.0%, with PPV, NPV, and accuracy values of 90.0%, 100.0%, and 94.0%, respectively, for the SUVmax analyses in the dynamic third phase and RI-SUVdyn. Compared with the AUC derived in all other ROC analyses, that for SUV3 was the largest at 0.967 ; however, Delong's test did not reveal any significant differences among the AUC values for all parameters ($p > 0.05$ for all).

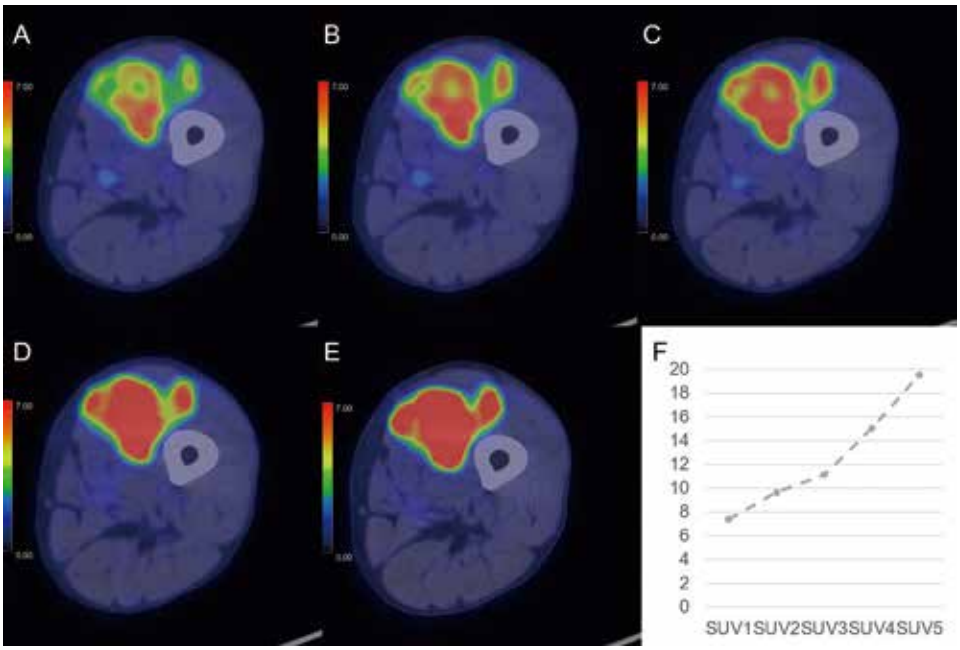

Fig 1. A 78-year-old woman with metastatic soft tissue tumor from gastric cancer in the left thigh
Positron emission tomography/computed tomography (PET/CT) (A-E) images are shown. On the dynamic phases (A-C), fluorodeoxyglucose (FDG) accumulation in the soft tissue tumor is inhomogeneous and focal intense accumulation is identifiable in the posterior part from the dynamic first phase (maximum standardized uptake value [SUVmax] : dynamic first phase, 7.41 ; dynamic second phase, 9.65 ; dynamic third phase, 11.14). The accumulation gradually becomes intense in most parts of the tumor during the dynamic phases (A-C). The 1-h early (D) and 2-h delayed (E) phases show homogeneous and intense accumulation in the soft tissue tumor (SUVmax: 1-h early phase, 15.04 ; 2-h delayed phase, 19.52). The time-SUVmax curve (F) shows a high level for the SUVmax for the dynamic first phase (SUV1), with a continuous increase during the dynamic (SUV1-3), 1-h early (SUV4), and 2-h delayed (SUV5) phases. The physiological FDG uptake of the bone and soft tissue in the early dynamic phase is faint, while the FDG accumulation in the tumor is clearly depicted.

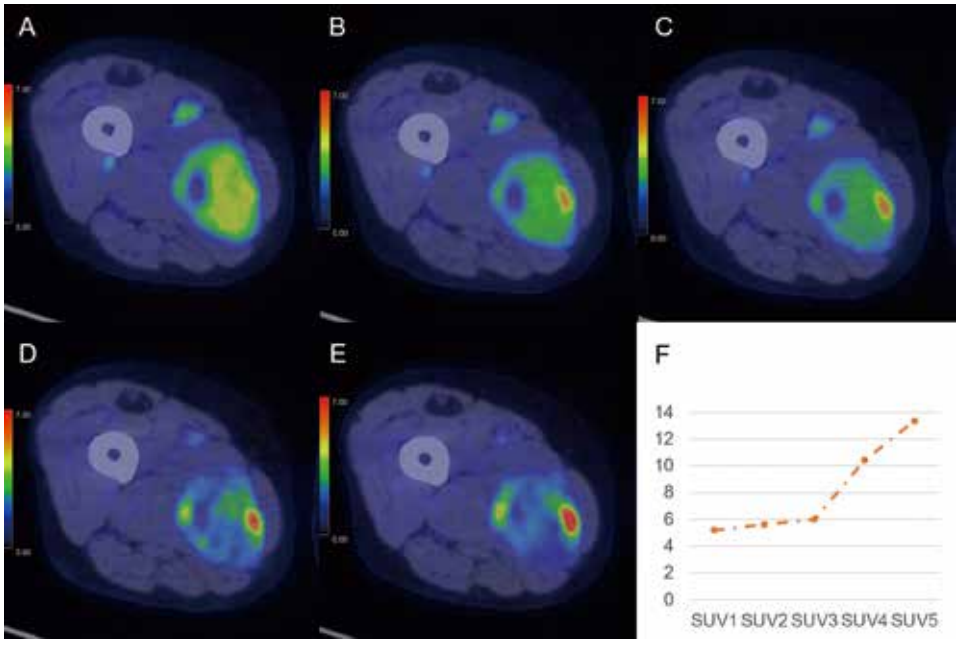

Fig 2. A 74-year-old-woman with differentiated liposarcoma (grade 2) in the right thigh
Positron emission tomography/computed tomography (PET/CT) images are shown for the dynamic (A-C), 1-h early (D), and 2-h delayed (E) phases. On the dynamic first phase (A), fluorodeoxyglucose (FDG) accumulation in the soft tissue tumor is inhomogeneous (maximum standardized uptake value [SUVmax], 5.21). After the dynamic second phase (B-E), the accumulation gradually becomes fainter and more homogeneous and the focal intense accumulation becomes clearer in the left portion of the tumor, compared with accumulation in the dynamic first phase (SUVmax : dynamic second phase, 5.63 : dynamic third phase, 6.02 : 1-h early phase, 10.41 : 2-h delayed phase, 13.35). The time-SUVmax curve (F) shows a gradual increase during the dynamic phases (SUV1-3) and a high level for the SUVmax during the 1-h early (SUV4) and 2-h delayed (SUV5) phases, with continuous increase.

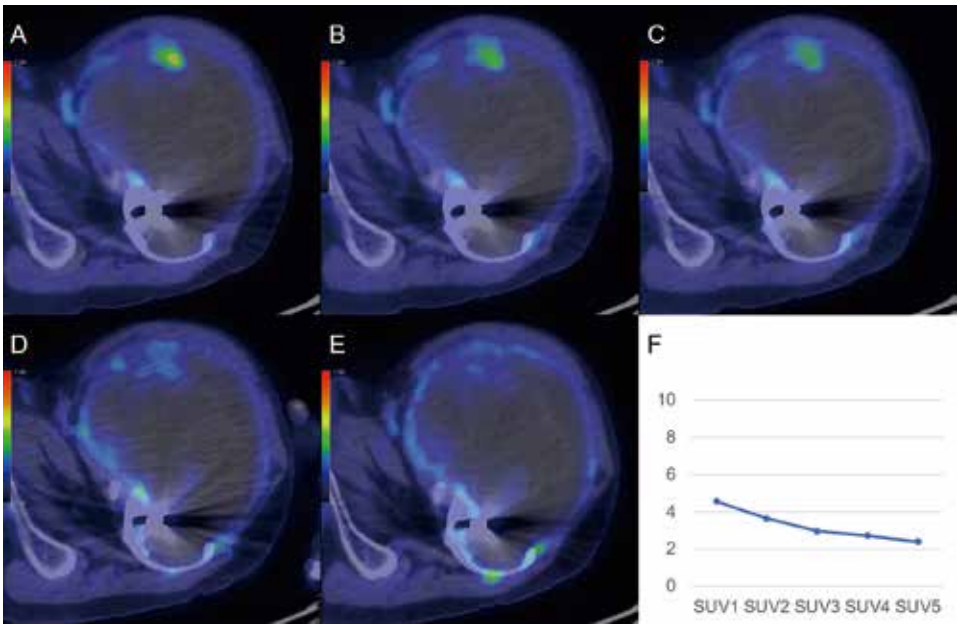

Fig 3. A 67-year-old-man with chronic expanding hematoma in the left femur
Positron emission tomography/computed tomography (PET/CT) images are shown for the dynamic (A-C), 1-h early (D), and 2-h delayed (E) phases. On the dynamic first phase (A), fluorodeoxyglucose (FDG) accumulation in the peripheral region of the bone tumor is focal and faint (maximum standardized uptake value [SUVmax], 4.57). After the dynamic second phase (B-E), FDG accumulation gradually becomes fainter (SUVmax : dynamic second phase, 3.65 : dynamic third phase, 2.97 : 1-h early phase, 2.73 : 2-h delayed phase, 2.40). The time-SUVmax curve (F) shows a low level for SUVmax at the dynamic first phase (SUV1), with a gradual decrease during the dynamic (SUV1-3), 1-h early (SUV4), and 2-h delayed (SUV5) phases.

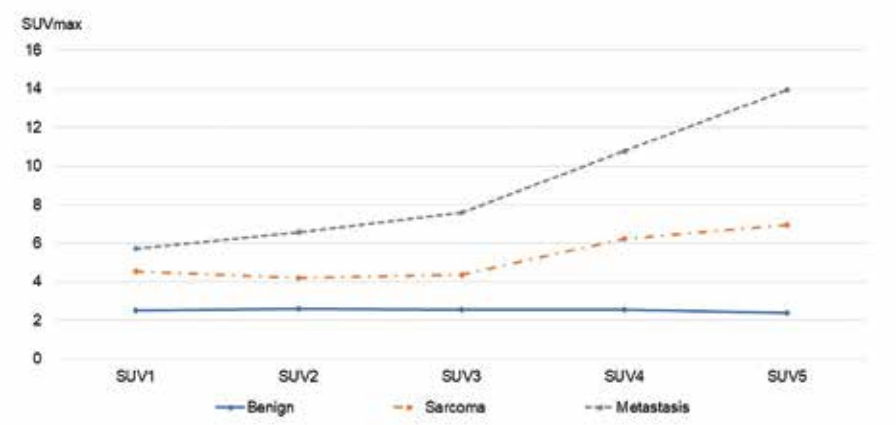

Fig 4. The change in median SUVmax values for each time phase in benign and malignant musculoskeletal lesions.

Table 4. Performance of various parameters in discriminating between MMSLs and BMSLs in semiquantitative analyses

	SUV1	SUV2	SUV3	SUV4	SUV5	RI-SUVdual
Threshold value	3.49	3.38	3.55	5.16	4.00	4.26
Sensitivity (%)	94.7	94.7	89.5	89.5	94.7	89.5
Specificity (%)	75.0	100.0	100.0	100.0	100.0	100.0
PPV (%)	94.7	94.7	100.0	100.0	100.0	100.0
NPV (%)	75.0	100.0	66.7	66.7	80.0	66.7
Accuracy (%)	91.3	95.7	91.3	91.3	95.7	91.3
AUC	0.895	0.987	0.974	0.980	0.961	0.908

SUV, standardized uptake value ; RI-SUV, retention index of maximum standardized uptake value ; dual, dual-time-point scans ; PPV, positive predictive value ; NPV, negative predictive value ; AUC, area under the curve ; MMSLs, malignant musculoskeletal lesions ; BMSLs, benign musculoskeletal lesions.

Table 5. Performance of various parameters in discriminating between MMSTs and PMMSTs in semiquantitative analyses

	SUV1	SUV2	SUV3	SUV4	SUV5	RI-SUVdyn
Threshold value	5.06	6.19	6.29	8.57	9.18	32.52
Sensitivity (%)	77.8	77.8	100.0	100.0	100.0	100.0
Specificity (%)	90.0	100.0	90.0	70.0	70.0	90.0
PPV (%)	87.5	100.0	90.0	75.0	75.0	90.0
NPV (%)	81.8	83.3	100.0	100.0	100.0	100.0
Accuracy (%)	84.2	89.5	94.7	84.2	84.2	94.7
AUC	0.833	0.933	0.967	0.856	0.856	0.956

RI-SUV, retention index of maximum standardized uptake value ; Dyn, dynamic scans ; PPV, positive predictive value ; NPV, negative predictive value ; AUC, area under the curve ; SUV, standardized uptake value ; PMMSTs, primary malignant musculoskeletal tumors ; MMSTs, metastatic musculoskeletal tumors.

DISCUSSION

To date, no studies have evaluated the diagnostic capabilities of dynamic ^{18}F-FDG PET/CT in differentiating between malignant and benign primary unknown MSLs. In this study, we assessed the changes in ^{18}F-FDG uptake in MSLs on dynamic PET/CT scans to compare their diagnostic capacity with that of DTP PET/CT scans. We also attempted to determine the phase that can provide the most accurate diagnostic information for MSLs.

In clinical functional imaging, the most popular method to diagnose malignancies is static PET imaging. The relatively weaker physiological accumulation of FDG in the bone and soft tissues, makes assessing the accumulation of FDG in musculoskeletal lesions easier compared to that in other organs. PMMSTs are typically ^{18}F-FDG-avid, while BMSLs show a faint ^{18}F-FDG uptake on static PET images. Reportedly, when using semiquantitative SUV-based methods in MSL cases, the utility of DTP scanning to evaluate FDG accumulation changes over time. In a prospective study of 67 patients with bone lesions (23), there were significant differences in SUVmax in the 1-h early phase and RI, with a sensitivity, a specificity, and an accuracy of 90.6%–96.0%, 44.0%–76.0%, and 72.4%–83.7%, respectively. The AUC values for RI were significantly greater than those for SUVmax in the 1-h early phase. In another study of 56 soft tissue tumors (24), there were significant differences in SUVmax between benign and malignant tumors on the 1-h early and 2-h delayed phases. However, low-grade malignant tumors show mild ^{18}F-FDG uptake and granulomas and active inflammation show false-positive findings on DTP scans (24, 25). Therefore, MSLs may show variable ^{18}F-FDG uptake, and conventional ^{18}F-FDG PET may have a limited role in the diagnosis of low-grade sarcomas and benign lesions (8, 26).

The present study showed transitional patterns of continually increasing ^{18}F-FDG uptake in most MMSLs and revealed that FDG avidity is stronger in MMSLs than in BMSLs from the early dynamic phase to the delayed phase. Especially, different from those for the BMSLs and PMMSTs, the SUVmax value in the dynamic second phase was higher than that in the dynamic first phase for all MMSTs. We found significant differences in the SUVmax for each time phase and RI-dyn between MMSTs and PMMSTs. In the included patients population, the median RI values for BMSLs were lower in the dynamic scans than in the DTP scans. According to a previous report, the SUVmax for 16 of 17 chronic bacterial osteomyelitis cases was stable or decreased between 30 and 90 min after injection, and the median SUVmax for 4 malignant lesions was 3.19 (range 2.31—4.70) at 30 min and 4.1 (range 3.52—5.32) at 90 min (26). Another report revealed a significant difference in the mean RI values between benign and malignant bone tumors on 2-h DTP scans (23). In the first few minutes after FDG injection, the FDG uptake is primarily determined by blood perfusion and vascular permeability in the specific tissue. In the subsequent metabolic phase, FDG is gradually accumulated in metabolically active cells (9). Our findings suggest that most MMSLs show progressively increasing FDG avidity from the early dynamic phase to the 2-h delayed phase and that FDG avidity is stronger at 5—35 min than at 60—120 min after injection. The amount of FDG metabolized in most MMSTs is greater than that metabolized in BMSLs and PMMSTs from the early dynamic phase, and it may be a key finding for differentiating between MMSTs and BMSLs and PMMSTs. FDG accumulation in BMSLs, except for granulomas, and active inflammation may continuously decrease or remain stable from the early dynamic phase.

Regarding differentiation between MMSLs and BMSLs, this study demonstrated a high diagnostic capacity for SUVmax cut-off value of 3.38, based on the ROC curve analysis of the dynamic second phase (AUC 0.987). In addition, although Delong's test did not reveal any significant differences among the AUC values for all parameters, ROC curve analysis for the dynamic third phase showed the highest diagnostic ability at the SUVmax cut-off value of 6.29 for differentiating MMSTs from PMMSTs (AUC 0.967). In dynamic PET studies without list-mode, the evaluation of full FDG kinetics and application of discriminant analysis are required and can be prospectively used to classify bone lesions as malignant or benign. A study (8) showed that this method had a sensitivity, a specificity, and an accuracy of 75.9%, 97.2%, and 87.7%, respectively. On ^{18}F-FDG PET studies in patients with MSLs, tumor heterogeneity, the number of granulomas, active inflammation, and low-grade sarcoma may affect the outcome of dynamic PET/CT imaging. Hence, our results suggest that the analysis of FDG accumulation in the early dynamic phases is a valuable predictor for discriminating MSLs and show that the diagnostic capacity of SUVmax on the dynamic second and third phases is equivalent or superior to that on the 1-h early and 2-h delayed PET/CT scans in our study population. Therefore, a diagnostic accuracy equal to that obtained using the 60-min and 120-min protocols used in clinical contexts can be obtained with a single measurement requiring 15–25 min. The diagnostic capacity of this approach alone may not be sufficient to differentiate between MSLs or be used as the basis for changing the current standard diagnostic flow, which is dependent on biopsy. However, the early dynamic PET/CT scans in list-mode may aid the prediction of histopathology in cases where it is impossible to

perform percutaneous biopsy and where there are multiple sites with various suspected morphological subtypes.

This study was limited by the small sample size and lack of granuloma and active inflammation cases, which show FDG avidity (false-positive) on routine FDG PET scans. Moreover, we did not assess the pathological background responsible for differences among MSLs in FDG uptake, which involves the expression of glucose transporters in the tumors, and did not perform kinetic modeling in FDG PET. A multi-institutional trial using a larger patient population that includes all histological subtypes, combined with a kinetic study and immunohistochemical analysis, may provide a clearer picture and more comprehensively reveal the diagnostic capacity of dynamic ^{18}F-FDG PET/CT scans for MSLs. Despite its limitations, this study demonstrated the high diagnostic ability of this approach for MMSLs and MMSTs with an optimal cut-off SUVmax. In addition, our dynamic ^{18}F-FDG PET/CT analysis can be routinely performed in clinical practice without additional invasive methods, such as continuous phlebotomy for arterial input function.

In conclusion, this study reported a transitional increase in the ^{18}F-FDG uptake in MMSLs and that FDG avidity was stronger in MMSLs than in BMSLs from the early dynamic phase to the 2-h delayed phase. In the included patients population, dynamic ^{18}F-FDG PET/CT, particularly when combined with semiquantitative analyses for SUV2 and SUV3, showed high diagnostic accuracy in differentiating between MSLs. Additional studies with larger cohorts are needed to identify the modality—dynamic PET/CT or DTP scanning—that performs better in terms of MSL differentiation.

CONFLICT OF INTERESTS

None

ACKNOWLEDGEMENTS

The authors would like to thank the radiographers and administration team at Tokushima University Hospital for their technical assistance and cooperation during the imaging and administration processes.

FUNDING

No funding was received for conducting the research or for reporting the results.

REFERENCES

1. Inai R, Shinya T, Tada A, Sato S, Fujiwara T, Takeda K, Kunisada T, Yanai H, Ozaki T, Kanazawa S : Diagnostic value of thallium-201 scintigraphy in differentiating malignant bone tumors from benign bone lesions. Ann Nucl Med 29 : 674-681, 2015
2. Keller S, Inai R, Sato S, Tada A, Adam G, Yamamura J, Kanazawa S : Thallium-201 uptake of giant cell tumor : One step toward the differential diagnosis to atypically presenting osteosarcoma. AJR Am J Roentgenol 208 : 171-179, 2017
3. Kobayashi H, Kotoura Y, Hosono M, Sakahara H, Hosono M, Yao ZS, Tsuboyama T, Yamamuro T, Endo K, Konishi J : Diagnostic value of Tc-99m (V) DMSA for chondrogenic tumors with positive Tc-99m HMDP uptake on bone scintigraphy. Clin Nucl Med 20 : 361-364, 1995
4. Choong PF, Kunisada T, Slavin J, Schlicht S, Hicks R : The role of thallium-201 and pentavalent dimercaptosuccinic acid for staging cartilaginous tumours. Int Semin Surg Oncol 1 : 10, 2004
5. Shinya T, Sato S, Kunisada T, Inai R, Yanai H, Ozaki T, Kanazawa S : Both a visual and a semiquantitative analysis for differentiating benign from malignant chondrogenic bone tumors using Tc-99m (V) DMSA scintigraphy : a prospective study. Nucl Med Commun 36 : 802-807, 2015
6. Hicks RJ : Functional imaging techniques for evaluation of sarcomas. Cancer Imaging 5 : 58-65, 2005
7. Dimitrakopoulou-Strauss A, Strauss LG, Schwarzbach M, Burger C, Heichel T, Willeke F, Mechtersheimer G, Lehnert T : Dynamic PET 18F-FDG studies in patients with primary and recurrent soft-tissue sarcomas : impact on diagnosis and correlation with grading. J Nucl Med 42 : 713-720, 2001
8. Dimitrakopoulou-Strauss A, Strauss LG, Heichel T, Wu H, Burger C, Bernd L, Ewerbeck V : The role of quantitative (18)F-FDG PET studies for the differentiation of malignant and benign bone lesions. J Nucl Med 43 : 510-518, 2002
9. Rusten E, Rødal J, Revheim ME, Skretting A, Bruland OS, Malinen E : Quantitative dynamic ^{18}FDG-PET and tracer kinetic analysis of soft tissue sarcomas. Acta Oncol 52 : 1160-1167, 2013
10. Okazumi S, Dimitrakopoulou-Strauss A, Schwarzbach MH, Strauss LG : Quantitative, dynamic 18F-FDG-PET for the evaluation of soft tissue sarcomas : relation to differential diagnosis, tumor grading and prediction of prognosis. Hell J Nucl Med 12 : 223-228, 2009
11. Dimitrakopoulou-Strauss A, Strauss LG, Egerer G, Vasamiliette J, Mechtersheimer G, Schmitt T, Lehner B, Haberkorn U, Stroebel P, Kasper B : Impact of dynamic 18F-FDG PET on the early prediction of therapy outcome in patients with high-risk soft-tissue sarcomas after neoadjuvant chemotherapy : a feasibility study. J Nucl Med 51 : 551-558, 2010
12. Dimitrakopoulou-Strauss A, Strauss LG, Egerer G, Vasamiliette J, Schmitt T, Haberkorn U, Kasper B : Prediction of chemotherapy outcome in patients with metastatic soft tissue sarcomas based on dynamic FDG PET (dPET) and a multiparameter analysis. Eur J Nucl Med Mol Imaging 37 : 1481-1489, 2010
13. Kwee TC, Basu S, Cheng G, Alavi A : FDG PET/CT in carcinoma of unknown primary. Eur J Nucl Med Mol Imaging 37 : 635-644, 2010
14. Schierz JH, Opfermann T, Steenbeck J, Lopatta E, Settmacher U, Stallmach A, Marlowe RJ : Early dynamic ^{18}F-FDG PET to detect hyperperfusion in hepatocellular carcinoma liver lesions. J Nucl Med 54 : 848-854, 2013
15. Nakajima R, Abe K, Kondo T, Tanabe K, Sakai S : Clinical role of early dynamic FDG-PET/CT for the evaluation of renal cell carcinoma. Eur Radiol 26 : 1852-1862, 2016
16. Epelbaum R, Frenkel A, Haddad R, Sikorski N, Strauss LG, Israel O, Dimitrakopoulou-Strauss A : Tumour aggressiveness and patient outcome in cancer of the pancreas assessed by dynamic ^{18}F-FDG PET/CT. J Nucl Med 54 : 12-18,2013
17. Belakhlef S, Church C, Jani C, Lakhanpal S : Early dynamic PET/CT and ^{18}F-FDG blood flow imaging in bladder cancer detection : a novel approach. Clin Nucl Med 37 : 366-368, 2012
18. Bernstine H, Braun M, Yefremov N, Lamash Y, Carmi R, Stern D, Steinmetz A, Sosna J, Groshar D : FDG PET/CT early dynamic blood flow and late standardized uptake value determination in hepatocellular carcinoma. Radiology 260 : 503-510, 2011
19. Shinya T, Otomi Y, Kubo M, Kinoshita M, Takechi K,

Uyama N, Yamanaka M, Terazawa K, Toba H, Bando Y, Otsuka H, Harada M : Preliminary clinical assessment of dynamic ^{18}F-fluorodeoxyglucose positron emission tomography/computed tomography for evaluating lymph node metastasis in patients with lung cancer : a prospective study. Ann Nucl Med 33 : 414-423, 2019

20. Shinya T, Otomi Y, Dimitrakopoulou-Strauss A, Kubo M, Kondo M, Otomo M, Terazawa K, Bando Y, Harada M : Preliminary clinical assessment of dynamic ^{18}F-fluorodeoxyglucose positron-emission tomography/computed tomography for evaluating the clinicopathological grade in patients with non-Hodgkin's lymphoma : a prospective study. Nucl Med Commun 41 : 26-33, 2020
21. Kanda Y : Investigation of the freely available easy-to-use software 'EZR' for medical statistics. Bone Marrow Transplant 48 : 452-458, 2013
22. Fletcher CDM, Bridge JA, Hogendoorn P, Mertens F : WHO Classification of Tumours of Soft Tissue and Bone. IARC Press, Lyon, 2013
23. Tian R, Su M, Tian Y, Li F, Li L, Kuang A, Zeng J : Dual-time point PET/CT with F-18 FDG for the differentiation of malignant and benign bone lesions. Skeletal Radiol 38 : 451-458, 2009
24. Hamada K, Tomita Y, Ueda T, Enomoto K, Kakunaga S, Myoui A, Higuchi I, Yoshikawa H, Hatazawa J : Evaluation of delayed 18 F-FDG PET in differential diagnosis for malignant soft-tissue tumors. Ann Nucl Med 20 : 671-675, 2006
25. Ishibashi M, Tanabe Y, Fujii S, Ogawa T : Pictorial review of ^{18}F-FDG PET/CT findings in musculoskeletal lesions. Ann Nucl Med 31 : 437-453, 2017
26. Sahlmann CO, Siefker U, Lehmann K, Meller J : Dual time point 2-[18F]fluoro-2'-deoxyglucose positron emission tomography in chronic bacterial osteomyelitis. Nucl Med Commun 25 : 819-823, 2004